Title
Infrared optical and thermal properties of microstructures in butterfly wings

Journal
Proceedings of the National Academy of Sciences of the United States of America, 117(3)

ISSN
0027-8424

Authors
Krishna, Anirudh
Nie, Xiao
Warren, Andrew D
et al.

Publication Date
2020-01-21

DOI
10.1073/pnas.1906356117

Peer reviewed

Infrared optical and thermal properties of microstructures in butterfly wings

Anirudh Krishna[a], Xiao Nie[a], Andrew D. Warren[b], Jorge E. Llorente-Bousquets[c], Adriana D. Briscoe[d], and Jaeho Lee[a,1]

[a]Department of Mechanical and Aerospace Engineering, University of California, Irvine, CA 92697; [b]McGuire Center for Lepidoptera and Biodiversity, Florida Museum of Natural History, University of Florida, Gainesville, FL 32611; [c]Museo de Zoología, Departamento de Biología Evolutiva, Facultad de Ciencias, Universidad Nacional Autónoma de México, 04510 Mexico City, Mexico; and [d]Department of Ecology and Evolutionary Biology, University of California, Irvine, CA 92697

Edited by Naomi J. Halas, Rice University, Houston, TX, and approved December 12, 2019 (received for review April 18, 2019)

While surface microstructures of butterfly wings have been extensively studied for their structural coloration or optical properties within the visible spectrum, their properties in infrared wavelengths with potential ties to thermoregulation are relatively unknown. The midinfrared wavelengths of 7.5 to 14 μm are particularly important for radiative heat transfer in the ambient environment, because of the overlap with the atmospheric transmission window. For instance, a high midinfrared emissivity can facilitate surface cooling, whereas a low midinfrared emissivity can minimize heat loss to surroundings. Here we find that the midinfrared emissivity of butterfly wings from warmer climates such as *Archaeoprepona demophoon* (Oaxaca, Mexico) and *Heliconius sara* (Pichincha, Ecuador) is up to 2 times higher than that of butterfly wings from cooler climates such as *Celastrina echo* (Colorado) and *Limenitis arthemis* (Florida), using Fourier-transform infrared (FTIR) spectroscopy and infrared thermography. Our optical computations using a unit cell approach reproduce the spectroscopy data and explain how periodic microstructures play a critical role in the midinfrared. The emissivity spectrum governs the temperature of butterfly wings, and we demonstrate that *C. echo* wings heat up to 8 °C more than *A. demophoon* wings under the same sunlight in the clear sky of Irvine, CA. Furthermore, our thermal computations show that butterfly wings in their respective habitats can maintain a moderate temperature range through a balance of solar absorption and infrared emission. These findings suggest that the surface microstructures of butterfly wings potentially contribute to thermoregulation and provide an insight into butterflies' survival.

microstructures | spectral emissivity | thermoregulation | butterflies

Structural origins of thermoregulation and color in nature have long been a topic of research for scientists and engineers (1, 2) studying, for example, feathers (3) in peacocks (4) and birds of paradise (5), the skins of squids (6–8) and chameleons (9), and coloration in plants (10–13) and insects, including silver ants (14–16). In the case of butterflies, coloration of wings arises from a combination of pigmentation and structural coloration by periodic chitin microstructures (17–19). For example, *Morpho* butterflies' vivid blue structural coloration is due to the scattering of light by tree-like microstructures of 1- to 1.5-μm-pitch branches and 0.15- to 0.2-μm-pitch lamellae (20–25). Gyroid microstructures provide coloration in butterfly wings as well (26). The vast array of different morphologies that give rise to structural coloration in butterfly wings can be modeled as periodic microstructures in most cases (27).

The role of periodic microstructures interacting with visible to near-infrared (near-IR) wavelengths of electromagnetic radiation leading to structural coloration has been studied extensively (20, 26–29). The interaction with visible to near-IR radiation also plays an important role in the heating of butterfly wings and bodies (18, 20, 30–34). Butterflies heat up their wings by absorbing the heat from the sun, in the ultraviolet (UV) to near-IR wavelengths of 0.3 to 2.5 μm. This heating is essential for facilitating thermoregulation in cold-blooded animals such as butterflies that rely on habitat, climate, behavioral changes, and evolutionary adaptations. Butterflies regulate their body temperature by controlling their activity level (18, 31, 35–37). Most butterflies are required to attain a body temperature of 20 to 50 °C, regardless of habitat, in order to be able to fly (38–40). At a body temperature less than 7 °C, all activity in the butterflies stops, and the same is also true for body temperatures above 50 °C (41).

In order to evaluate the heating of butterfly wings and quantify the absorption of solar radiation, Munro et al. (32) analyzed the optical behavior of butterfly wings up to a wavelength of 1.1 μm, encompassing roughly 83% of the incoming solar spectrum. Analyzing the optical properties over the entire solar spectrum up to 2.5-μm wavelength could provide a fuller understanding of the heating of the butterfly wings, as has been suggested by Bosi et al. (33). However, the existing literature analyzing solar absorption provides an incomplete thermal analysis, as it does not account for the mid-IR optical properties of the butterfly wings.

The use of thermoregulation to maintain a body temperature in the 20 to 50 °C range in butterflies is not just limited to absorption of solar heat. Butterflies also emit heat from their wings, providing a heat loss mechanism. Most terrestrial beings emit heat from their surface within the mid-IR wavelengths of 7.5 to

Significance

The optical properties of microstructures on butterfly wings are well studied in the visible spectrum, providing an understanding of the origins of structural coloration. Meanwhile, there is a need for evaluating their midinfrared optical properties, due to the critical role these properties play in thermoregulation. While a high visible absorptivity offers heating by absorption of solar radiation, a high midinfrared emissivity offers heat loss via thermal emission. Here we evaluate the midinfrared optical properties of 4 butterfly species from different habitats and analyze the effect of this emissivity on wing temperature. With the wing temperatures attaining similar values irrespective of their habitats of origin, our findings demonstrate the potential influence of butterfly wing microstructures on midinfrared optical properties and thermoregulation.

Author contributions: A.K. and J.L. designed research; A.K. and X.N. performed research; A.D.W. and J.E.L.-B. provided habitat information; A.K., X.N., A.D.B., and J.L. analyzed data; A.K., A.D.B., and J.L. wrote the paper; and A.D.W., J.E.L.-B., and A.D.B. collected the butterfly specimens and identified them.

The authors declare no competing interest.

This article is a PNAS Direct Submission.

Data deposition: Spectroscopic data, thermal measurements, and related codes used in the work are available at DOI 10.17605/OSF.IO/F8RN7.

[1]To whom correspondence may be addressed. Email: jaeholee@uci.edu.

This article contains supporting information online at https://www.pnas.org/lookup/suppl/doi:10.1073/pnas.1906356117/-/DCSupplemental.

First published January 9, 2020.

14 μm as described by Wien's Law (42). Earth's atmosphere is also highly transmissive in the same spectral range (36, 37). A high emissivity in the mid-IR wavelengths would thus increase heat loss via thermal emission by the butterfly wings and lower their temperature. Similarly, heat loss can be minimized with low emissivity in the mid-IR wavelengths, maintaining the temperature of the wings.

While visible coloration and solar absorption characteristics have been extensively studied in butterflies (2, 17, 22, 23, 28), their mid-IR optical properties and thermoregulation have not (18, 43). Butterfly wings also scatter mid-IR radiation apart from UV, visible (Vis), and near-IR radiation (43). This could be due to the presence of unique microstructures that specifically interact with the mid-IR wavelengths. To effectively regulate their wing temperatures, butterflies may have evolved microstructures that affect their solar absorptivity and mid-IR emissivity (18, 33, 44–46). Analyzing the role of microstructures in thermoregulation could enhance our understanding of the survival mechanisms of butterflies.

We analyze 4 species (*Archaeoprepona demophoon mexicana*, *Celastrina echo sidara*, *Heliconius sara sprucei*, and *Limenitis arthemis astyanax*) from distinct geographical regions ranging from the Ecuadorian rainforests to the Front Range of Colorado's Rocky Mountains. The varying geography is also accompanied by climatic variation ranging from hot and humid in the rainforests to the mountainous cold climates. *A. demophoon* is found in Oaxaca, Mexico, through the year, where the air temperature remains around 20 to 35 °C (warm/dry) (47). *C. echo* is found in abundance in the Rocky Mountains in Colorado between the months of April and July, with air temperatures between 10 and 25 °C (cool/dry) (47). *H. sara* is found in Ecuador throughout the year, where the air temperatures are between 25 and 35 °C (warm/humid) (48). *L. arthemis* is found in Florida in abundance from March to October, where the air temperatures are around 15 to 30 °C (moderate/humid) (48). The 4 species could thus serve as arbiters for species from differing climatic and geographical conditions. These 4 species also lack optical data in the mid-IR spectrum, and have not been evaluated for their thermoregulation. With measured and computed optical data, we performed analytical computations and measurements of the thermal performance of these specimens to analyze their behavior both in the temperatures of their respective habitats and when placed in a uniform control environment.

Results

Scanning Electron Microscopy of Butterfly Wings. The periodic microstructures present in the butterfly wings were analyzed using scanning electron microscopy (SEM) imaging with a Philips XL-30 microscope of the right dorsal hindwing of each specimen. The images shown in Fig. 1 depict the mesh-like microstructures present on the wing scales of the butterfly specimens. These microscale meshes contain periodic ridges linked together by cross-links in the transverse direction.

Periodic microstructures have been hypothesized to correspond to structural coloration of butterfly wing scales (17–20, 23, 28, 49). Hence, we compared the SEM images from various locations on the butterfly wing specimens (*SI Appendix*, Fig. S1). From optical imaging, *A. demophoon* and *L. arthemis* wings have distinct structurally colored regions, while *H. sara* appears mostly blue except for the edge of the wing. *C. echo* displays uniform visible coloration. Under SEM imaging, however, the varying regions of the wing all display periodic mesh-like microstructures across the varying colored regions (*SI Appendix*, Fig. S1).

The dimensions for the ridge periodicity (a), cross-link periodicity (b), ridge thickness (c), and cross-link thickness (d) were measured from the SEM images and are reported with their respective SD values from measurements at 100 locations across multiple scales for each specimen (Fig. 1). The dimensional parameters vary across the different species, with a ranging between 1 and 2 μm, b ranging between 0.5 and 1 μm, c between 0.25 and 0.5 μm, and d at 0.2 μm. The parameter e was taken from measurements of angled SEM images of the specimens (*SI Appendix*, Fig. S2), with $e = 1.2 \pm 0.1$ μm, and is comparable to the existing literature (50–52). The biological nature of the specimens presents an inherent natural variation in the structural parameters ranging between 0.01 and 0.2 μm, and could lead to broadband optical and thermal control (53–55) (*SI Appendix*, Fig. S3).

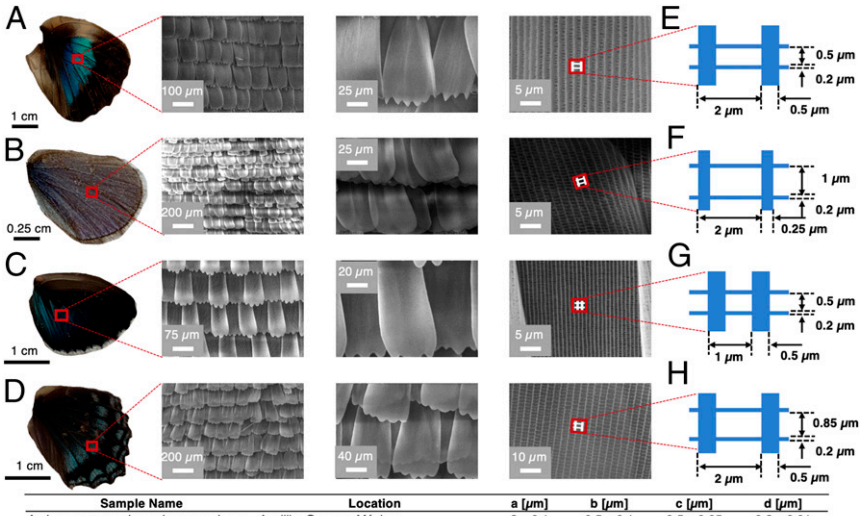

Sample Name	Location	a [μm]	b [μm]	c [μm]	d [μm]
Archaeoprepona demophoon mexicana	Azulillo, Oaxaca, México	2 ± 0.1	0.5 ± 0.1	0.5 ± 0.05	0.2 ± 0.01
Celastrina echo sidara	Sugar Creek, Colorado, U.S.A.	2 ± 0.1	1 ± 0.2	0.25 ± 0.05	0.2 ± 0.01
Heliconius sara sprucei	Unión del Toachi, Pichincha, Ecuador	1 ± 0.1	0.5 ± 0.1	0.5 ± 0.05	0.2 ± 0.01
Limenitis arthemis astyanax	Bronson, Florida, U.S.A.	2 ± 0.1	0.85 ± 0.2	0.5 ± 0.05	0.2 ± 0.01

Fig. 1. Optical images and SEM images for the right dorsal hindwings from (*A*) *A. demophoon*, (*B*) *C. echo*, (*C*) *H. sara*, and (*D*) *L. arthemis*. The images depict the presence of periodic microstructures on the wing scales of the butterflies. The periodic microstructures are present as mesh-like features with prominent ridges and cross-links that traverse the ridges (depicted as *Inset* schematics). (*E*–*H*) The microstructures are modeled as a unit cell based on dimensions from the SEM images.

Optical Properties of Butterfly Wings. Spectroscopy on the butterflies was carried out on the right dorsal hindwing of individual specimens of *A. demophoon* ($n = 5$), *C. echo* ($n = 4$), *H. sara* ($n = 4$), and *L. arthemis* ($n = 9$) (56). The measurements provide the emissivity [and, consequently, the absorptivity, assumed equal to the emissivity by Kirchhoff's Law (42)] as unity minus the sum of the reflectivity and transmissivity (42, 57) (Fig. 2).

The UV/Vis spectroscopy yields absorptivity/emissivity dips (and, hence, reflectivity peaks; *SI Appendix*, Fig. S4) for *A. demophoon* (with a reflectivity peak of 0.26 centered at 0.4 μm), *H. sara* (reflectivity peak of 0.11 around 0.37 to 0.41 μm), and *L. arthemis* (reflectivity peak of 0.32 between 0.38 and 0.42 μm), with a near-uniform reflectivity of 0.33 for *C. echo*. The solar absorptivity allows for absorption of incident solar irradiation to aid in heating of the butterflies by absorption of incident solar irradiation (30). We observed moderately high solar absorptivity values for all 4 species (>0.5) within the Vis spectrum (0.3 to 0.7 μm), slowly tapering down to 0.2 to 0.6 as the near-IR wavelength regions are approached (Fig. 2*A*). The average solar absorptivity of the specimens contains an uncertainty of ±0.03 for *A. demophoon* and *C. echo*, ±0.05 for *H. sara*, and ±0.04 for *L. arthemis*.

The mid-IR emissivity values were then recorded by Fourier-transform IR (FTIR) measurements (*SI Appendix*, Fig. S5). While the mid-IR emissivity in the wavelengths of 8 to 14 μm remained at 0.2 to 0.3 for *C. echo* and *L. arthemis*, *A. demophoon* and *H. sara* showed a mid-IR average emissivity of 0.4 to 0.6 (Fig. 2*B*). The average mid-IR emissivity of the specimens contains an uncertainty of ±0.03 for *A. demophoon*, ±0.02 for *C. echo*, and ±0.05 for *H. sara* and *L. arthemis*. There are prominent emissivity peaks in the wavelengths of 3 and 6 μm due to the presence of chitin (43) (*SI Appendix*, Fig. S7), seen across all butterfly specimens. The mid-IR wavelengths of 7.5 to 14 μm are critical for thermoregulation by means of mid-IR heat loss (58–61). Changes in thermal performance of butterfly wings by varying mid-IR emissivity as observed here might aid in thermoregulation of the butterflies.

Validation of Mid-IR Emissivity by IR Thermography. Next, we sought to validate the FTIR measurements of mid-IR emissivity by using IR thermography to measure the average mid-IR emissivity of the butterfly wing specimens between the wavelengths of 7.5 and 14 μm (*SI Appendix*, Fig. S6). The spectral average mid-IR emissivity values from IR thermography range from a low of 0.24 ± 0.04 for *C. echo* to a high of 0.52 ± 0.05 for *H. sara*, with intermediate values of 0.33 ± 0.04 for *L. arthemis*, and 0.42 ± 0.05 for *A. demophoon*. The IR thermography results were then compared with the average emissivity (in the 7.5- to 14-μm-wavelength range) taken from FTIR spectroscopy and showed similar values (Fig. 3).

The IR imaging in Fig. 3 depicts nearly uniform mid-IR emissivity across the right dorsal hindwing specimens, measured as a function of the perceived temperature on the IR map. On the *A. demophoon* wing, we noticed regions of lower emissivity closer to the proximal region, with a nearly uniform higher emissivity present toward the edge of the wing. For the *C. echo* wing, we observed a near-uniform low emissivity across the specimen, with a near-uniform high emissivity on the *H. sara* wing barring high emissivity black regions closer to the wing hinge. The *L. arthemis* wing depicts minimal variation in emissivity across the wing moving from the hinge to the edge. The IR imaging thus depicts no clear mid-IR distinction across the visibly distinct colored regions of the specimens (*SI Appendix*, Fig. S5), and indicates the possibility that different microstructures are responsible for thermoregulation and coloration. The measurement of mid-IR emissivity by IR imaging at a temperature of 69 to 70 °C yields comparable results to the FTIR spectroscopy done at 20 to 22 °C, depicting negligible variation of optical properties with changes in specimen temperature.

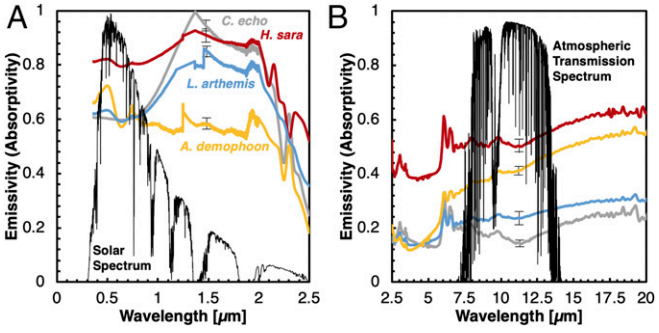

Fig. 2. Spectral emissivity (absorptivity) values for the butterfly wing specimens (right dorsal hindwing). (*A*) UV/Vis spectroscopy for *A. demophoon* (yellow), *H. sara* (red), *C. echo* (gray), and *L. arthemis* (blue) measures the spectral emissivity in the wavelength range of 0.3 to 2.5 μm. The results depict moderately high emissivity (absorptivity) values throughout the UV/Vis spectrum, with the average values being around 0.82 for *H. sara*, 0.69 for *C. echo*, 0.67 for *L. arthemis*, and 0.55 for *A. demophoon*. (*B*) FTIR spectroscopy performed in the wavelength range of 2.5 to 20 μm to evaluate the mid-IR emissivity (absorptivity) profiles for the butterfly wing specimens. The results depict mid-IR (7.5 to 14 μm) emissivity (absorptivity) values ranging from around 0.54 for *H. sara* (red), 0.42 for *A. demophoon* (yellow), 0.3 for *L. arthemis* (blue), and 0.18 for *C. echo* (gray), in decreasing order. The spectra are depicted with an overlay of the atmospheric transmission spectrum (7.5 to 14 μm) which aids in reemission of heat to outer space and, consequently, heat loss (58).

Optical Computations. Using the microstructures obtained from the SEM imaging of the butterfly wing specimens (Fig. 1), we evaluated the spectral absorptivity/emissivity for the specimens by rigorous coupled-wave analysis (RCWA) (61–63), with custom-modified open-source code (61–63). The geometric dimensions for computation were gathered from the SEM images as shown in Fig. 1, and the refractive index and extinction coefficient of chitin were taken from the literature (43, 64, 65). The natural variations and disorder in the structural parameters (*SI Appendix*, Fig. S3) do not permit perfect periodicity, and hence we used the measured average of each of the geometric dimensions of the microstructures in order to impose periodicity.

The RCWA results for each of these specimens depict mid-IR emissivity values ranging between 0.2 and 0.6, show similar optical behavior across the computation and spectroscopic measurements, and demonstrate the suitability of using a unit cell approximation to model the butterfly wing microstructures (Fig. 4). The results were also compared with finite-difference time-domain (FDTD) methods (66) (*SI Appendix*, Fig. S7*B*) for validation.

Thermal Properties of Butterfly Wings. We comparatively evaluated the steady state temperatures attained by the wings under a control environment to analyze the effects of structural thermoregulation. The measurements were performed between 9 AM and 3 PM on July 31, 2018, with the air temperature ranging from 20 to 27 °C, wind speeds between 0.26 and 0.44 $m \cdot s^{-1}$, and a near-constant humidity of 46 to 48%.

Our wing temperature measurements using an FLIR A655sc IR camera (Fig. 5*C*) showed a wing temperature of 36 to 38 °C for *A. demophoon*, with *C. echo* attaining 42 to 45 °C at 12 noon (56). The temperature of the specimens was also predicted using an energy balance analysis (59, 61, 67), with the specimens exposed to solar irradiation ($P_{sun''}$) and heat radiated from the atmosphere ($P_{atm''}$) = $\int \cos\theta \; d\Omega \int_0^\infty I_{BB}(T,\lambda)\varepsilon(\lambda,\Omega)\varepsilon_{atm}(\lambda,\Omega)\, d\lambda$ (I_{BB}: blackbody radiation; ε: emissivity of the specimen and the atmosphere (*atm*); θ: zenith angle [taken to be 30° on average]; Ω: solid angle interacting with the specimen surface). The specimens

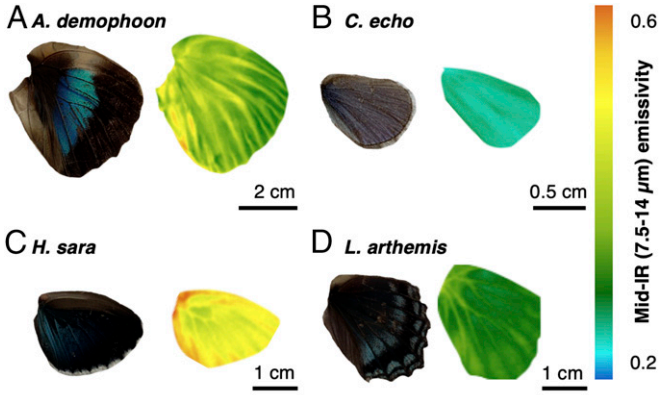

Sample	FTIR (7.5-14 μm)	IR Thermography
A. demophoon	0.42 ± 0.03	0.37 ± 0.05
C. echo	0.18 ± 0.02	0.24 ± 0.04
H. sara	0.54 ± 0.05	0.52 ± 0.05
L. arthemis	0.3 ± 0.05	0.33 ± 0.04

Fig. 3. Comparison of average mid-IR emissivity for various right dorsal hindwing specimens between the wavelengths of 7.5 and 14 μm using IR thermography and FTIR measurements for (*A*) *L. arthemis*, (*B*) *C. echo*, (*C*) *H. sara*, and (*D*) *A. demophoon*. The IR mapping presented here depicts variations in emissivity values across the wing specimens, with lower emissivity regions moving toward the blue colors on the map, and higher emissivity regions moving toward the red. While *C. echo* depicts an average mid-IR emissivity of 0.24, the values remain at 0.33 for *L. arthemis* and at 0.42 for *A. demophoon*, and reach a value of 0.54 for the *H. sara*. The uncertainty of the measured emissivity values includes the uncertainty in the measurement temperature and the inherent uncertainty of the instrument itself. The results for the 4 species depict close similarity in values for the different methods and validate the measurement observations.

emit radiation to outer space at 3 K (via the atmospheric transmission window) with $P_{rad}{''} = \int\cos\theta\, d\Omega \int_0^\infty I_{BB}(T,\lambda)\varepsilon(\lambda,\Omega)\, d\lambda$, and exchange heat with the environment via conduction and convection ($P_{cond+conv}{''} = h_{eff}(T–T_{air})$; h_{eff}: effective heat transfer coefficient; T_{air}: ambient air temperature). This gives a net radiative power ($P_{net}{''}$), given by Eq. **1** (59, 61, 67), of

$$P_{rad}{''}(T) - P_{atm}{''}(T_{air}) - P_{sun}{''} + P_{cond+conv}{''} = P_{net}{''}. \qquad [1]$$

The net heat flux into the specimens at an ambient air temperature of 27 °C at 12 noon ($P_{sun}{''} + P_{atm}{''}$) was computed to be 575 W·m^{-2} for *A. demophoon*, 642 W·m^{-2} for *C. echo*, 786 W·m^{-2} for *H. sara*, and 613 W·m^{-2} for *L. arthemis*. The net heat flux out of the specimens at an ambient air temperature of 27 °C at 12 noon ($P_{rad}{''}$) was computed to be 320 W·m^{-2} for *A. demophoon*, 276 W·m^{-2} for *C. echo*, 538 W·m^{-2} for *H. sara*, and 270 W·m^{-2} for *L. arthemis*. The sum of the net heat flux into and out of the specimens gives the net heat flux required to maintain the specimen at its steady-state temperature from the ambient temperature. The steady-state temperature of the specimen is attained when the sum of all heat fluxes for the specimen is zero. The steady-state temperatures of the specimens were then compared with the measured values (Fig. 5*C*). *C. echo* and *L. arthemis*, in general, heat up throughout the day consistently higher than *A. demophoon* and *H. sara* under similar ambient conditions in a controlled environment. The relatively lower wing temperature values for the warmer climate butterflies *A. demophoon* and *H. sara* thus depict the effects of mid-IR heat losses by periodic microstructures in the butterfly wings.

We also predicted the steady-state temperatures attained by the wings in their respective habitats, with the temperature and solar irradiation data taken for July over the past decade (2007–2017) (47, 48, 68, 69) in Santa María Huatulco, Oaxaca, Mexico, for *A. demophoon* (70), and Deckers, CO, for *C. echo* (47, 48). The temperature data were also compared with other weather stations within their habitats, such as Azulillo, Oaxaca, Mexico, and Estes Park, CO (48, 71) (*SI Appendix*, Figs. S8 and S9). While inherent variation in data exists across multiple sources, the sources we used are considered reliable and should account for locational variation. The data are thus expected to accurately depict the thermal environment of the butterflies, barring other sources of variation in their thermal microhabitat as discussed below. The specimens were assumed to be exposed to incident solar irradiation ($P_{sun}{''}$) taken to be varying at 580 to 1,000 W·m^{-2} for each location correspondingly. While the butterflies' habitats may offer forest cover or other obstacles to solar irradiation,

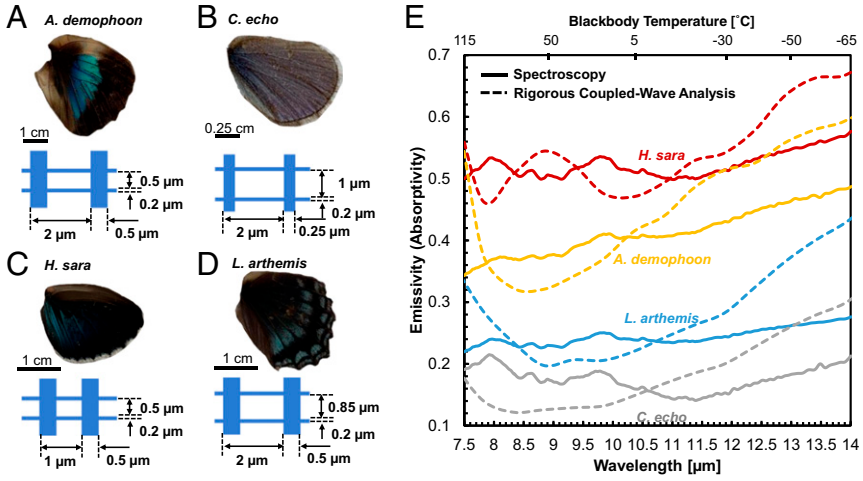

Fig. 4. Experimental and computational emissivity data between 7.5 and 14 μm wavelengths (within the atmospheric transmission spectrum) for the sample butterfly species (with schematics for the specimens) for (*A*) *A. demophoon*, (*B*) *H. sara*, (*C*) *C. echo*, and (*D*) *L. arthemis*. (*E*) The emissivity values are computed using RCWA based on structural dimensions (*A*–*D*) from SEM imaging. The emissivity values are plotted with respect to the wavelength and corresponding blackbody temperature [calculated using the Wien's displacement law (75)]. Both the measured and computed emmisivity values indicate distinct differences among the four butterfly species.

the butterflies generally bask under direct sunlight (31, 72, 73), and, as such, the forest cover can be assumed to have minimal effect on the incident solar radiation. The specimens interact with the surroundings by means of convective and conductive losses ($P_{cond+conv}''$), with h_{eff} taken to be 5 $W{\cdot}m^{-2}{\cdot}K^{-1}$ (for calm air), 10 $W{\cdot}m^{-2}{\cdot}K^{-1}$ (for a gentle breeze), or 20 $W{\cdot}m^{-2}{\cdot}K^{-1}$ (for a strong breeze). Increasing convection from the wings to the surrounding air for both butterflies would result in surface temperatures that gradually approach the air temperature. We computed the net radiative power (P_{net}'') using Eq. **1** (61).

The calculations (Fig. 5 *D* and *E*) show a steady-state wing temperature of 47 to 51 °C attained by both specimens with respect to their corresponding habitats at 12 noon with peak solar irradiance. The temperatures remained within 20 to 50 °C and likely aid in survival by thermoregulation (30, 34, 36). The analysis predicts the upper limit for daytime wing temperature, as it assumes clear skies, and overpredicts nighttime radiative losses by assuming the entire dorsal wing is exposed to the cold sky. The actual butterflies at nighttime are likely perched under leaves, within rock crevices, in clusters, or with the dorsal side of the wings hidden (37, 74).

The present study analyzes the steady-state wing temperatures of the butterflies at rest. During flight, the energy balance is expected to differ from the rest condition, due to changes in the thermal processes associated with the butterflies. While the major changes involve variations in convection, there is also the possibility of metabolic heat generation (72), and other related thermal processes. Flight is expected to increase the convection coefficient (h) for the butterflies, due to increase in associated wind velocity over the wings, leading to possible lowering of wing temperatures (Fig. 5 *D* and *E*). For example, an increase in the h from 10 $W{\cdot}m^{-2}{\cdot}K^{-1}$ to 20 $W{\cdot}m^{-2}{\cdot}K^{-1}$ leads to a decrease in the wing temperature for *A. demophoon* and *C. echo* from 50 to 51 °C to 40 to 44 °C. Meanwhile, the flight activity itself could lead to increased metabolism and, correspondingly, a possible increase in the butterflies' temperatures. The temperature prediction for butterfly wings during flight requires further investigations and transient heat transfer analysis with information about convection and metabolic properties (73).

Discussions

The mid-IR emissivity values for the butterfly wing microstructures range from high to low, roughly corresponding to the habitat temperature for the butterflies ranging from warm to cool. The results illustrate the role played by periodic microstructures on butterfly wings' mid-IR optical properties, and their impact on butterfly thermoregulation. Further evaluation of the correlation of habitat temperature with solar and mid-IR optical properties of butterfly wings would likely advance our understanding of how butterflies adapt to varying habitat environments. For instance, the current study depicts warmer climate butterflies with increased mid-IR emissivity values. Meanwhile, existing literature indicates increased flight duration for butterflies from warmer climates (73). The link between the warmer climates, increased mid-IR emissivity, and increased flight duration could possibly be explained due to the decreased thermalization time for increased mid-IR emissivity. However, the hypothesis would require further analysis to yield conclusive results.

Apart from butterflies, studies on the structural thermoregulation of other geographically and climatically diverse animals could lead to better insights as to the role of IR optical properties in the ability of organisms to adapt to their surroundings. For instance, insects such as ants are widespread and found in extreme climates. Analysis of the mid-IR optical properties in such ants could enhance our understanding of the role of structural thermoregulation in their survival and dispersal.

The natural variations in the structural parameters of the microstructures could also act as a basis for the development of bioinspired designs for broadband thermal control. Unlike the narrowband requirements of photonic systems, thermal systems favor broadband properties that do not require perfectly periodic structures, making the butterfly wing microstructures potential candidates for the design of thermal control systems. Our results thus present an improved knowledge of surface microstructures in nature and their relationship to thermoregulation.

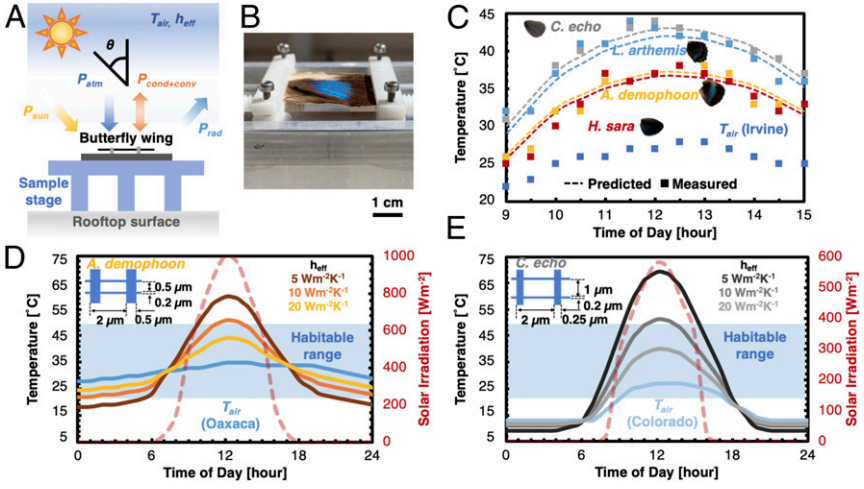

Fig. 5. Thermal analysis of butterfly wings. (*A*) Schematic of temperature measurement setup under a control environment with the energy balance considered for the thermal analysis, including incoming heat from the sun and atmosphere, outgoing radiation to outer space, and conductive and convective losses. (*B*) Optical image of temperature measurement on the *A. demophoon* right dorsal hindwing specimen. The specimen is held with clamps placed on a specimen holder mounted on thermal isolation legs. (*C*) Measured temperature comparison of the 4 specimens of butterflies under similar ambient climate conditions in a control environment (Irvine, CA) on July 31, 2018. While *A. demophoon* (yellow) and *H. sara* (red) attained wing temperatures of 37 °C at noon, *C. echo* (gray) and *L. arthemis* (blue) heated up further to 41 to 42 °C, highlighting the role of mid-IR heat losses in warmer climate butterflies. The measurements are validated by computational temperature predictions. (*D* and *E*) Theoretical predictions of the butterfly wing temperatures in their respective habitat conditions for the 2 species, (*D*) *A. demophoon* and (*E*) *C. echo*, depicting a surface temperature of 47 to 51 °C [within the habitable range of 20 to 50 °C (30, 34, 35)] with an effective heat transfer coefficient of 10 $W{\cdot}m^{-2}{\cdot}K^{-1}$ (a gentle breeze) at 12 noon. The habitat air temperatures were taken as an average in July for the past decade (2007–2017) and the dashed lines representing the incident solar irradiation (47).

Methods

Spectroscopic data, thermal measurements, and related codes used in the work are available at DOI 10.17605/OSF.IO/F8RN7.

Specimen Collection. Male butterflies were collected from Sugar Creek, CO (*C. echo sidara*) in 2008, Azulillo, Oaxaca, México *(A. demophoon mexicana*) in 2008 and 2012, Unión del Toachi, Pichincha, Ecuador *(H. sara sprucei*) in 2011, and Bronson, FL (*L. arthemis astyanax*) in 2016 and 2018. Wings were removed and stored in glassine envelopes in the dark.

Measurement of Optical Properties. The optical properties of the butterfly wing specimens in the UV to NIR wavelengths were characterized using the Cary 7000 Universal Measurement Spectrometer and the Jasco V-670 with a 60-mm integrating sphere. The inherent uncertainty in the optical properties is $\pm$0.003, with the wavelength uncertainty being $\pm$0.3 nm at a stable room temperature of 20 °C. In the mid-IR wavelengths, the optical properties of the specimens were characterized using Jasco 4700 and Thermo Nicolet 6700 spectrometers. The uncertainty in wavelength during measurement is $\pm$0.03 μm.

For the IR thermography, we used an FLIR A655sc IR camera. The specimen was placed on a reflective surface on a heated stage at 69 to 70 °C and secured in place with an IR transmissive, AR-coated ZnSe lens. The average mid-IR emissivity of the specimens was then measured by variation of the emissivity (an input parameter) to match the temperature of the specimen. The resolution of the IR camera is 0.03 K with an inherent uncertainty of $\pm$0.5 K for a measurement range of 273 to 343 K.

ACKNOWLEDGMENTS. A.K. and X.N. thank Dr. Q. Lin/Irvine Materials Research Institute and Dr. D. Fishman/Laser Spectroscopy Laboratory for training with the SEM and spectroscopy, and members of the Nano Thermal Energy Research laboratory for reading the manuscript. This work was partially supported by NSF Grants DEB-1342759 and IOS 1656260 to A.D.B., Programa de Apoyo a Proyectos de Investigación e Innovación Tecnológica Grant 212418 to J.E.L.-B., and by startup funds from the Henry Samueli School of Engineering at the University of California, Irvine and the Hellman Faculty Fellowship to J.L.

1. S. Kinoshita, *Structural Colors in the Realm of Nature* (World Scientific, 2008).
2. J. Sun, B. Bhushan, J. Tong, Structural coloration in nature. *RSC Advances* **3**, 14862–14889 (2013).
3. C. W. Mason, Structural colors in feathers. II. *J. Phys. Chem.* **27**, 401–448 (1923).
4. J. Zi *et al*., Coloration strategies in peacock feathers. *Proc. Natl. Acad. Sci. U.S.A.* **100**, 12576–12578 (2003).
5. D. E. McCoy, T. Feo, T. A. Harvey, R. O. Prum, Structural absorption by barbule microstructures of super black bird of paradise feathers. *Nat. Commun.* **9**, 1 (2018).
6. K. M. Cooper, R. T. Hanlon, B. U. Budelmann, Physiological color change in squid iridophores. II. Ultrastructural mechanisms in *Lolliguncula brevis*. *Cell Tissue Res.* **259**, 15–24 (1990).
7. N. W. Roberts, N. J. Marshall, T. W. Cronin, High levels of reflectivity and pointillist structural color in fish, cephalopods, and beetles. *Proc. Natl. Acad. Sci. U.S.A.* **109**, E3387 (2012).
8. S. Vignoli, U. Steiner, B. J. Glover, Reply to Roberts et al.: Reflectivity and pointillist structural color on land and in water. *Proc. Natl. Acad. Sci. U.S.A.* **109**, E3388 (2012).
9. J. Teyssier, S. V. Saenko, D. van der Marel, M. C. Milinkovitch, Photonic crystals cause active colour change in chameleons. *Nat. Commun.* **6**, 6368 (2015).
10. H. M. Whitney *et al*., Floral iridescence, produced by diffractive optics, acts as a cue for animal pollinators. *Science* **323**, 130–133 (2009).
11. H. M. Whitney, M. Kolle, R. Alvarez-Fernandez, U. Steiner, B. J. Glover, Contributions of iridescence to floral patterning. *Commun. Integr. Biol.* **2**, 230–232 (2009).
12. B. J. Glover, H. M. Whitney, Structural colour and iridescence in plants: The poorly studied relations of pigment colour. *Ann. Bot.* **105**, 505–511 (2010).
13. E. Moyroud *et al*., Disorder in convergent floral nanostructures enhances signalling to bees. *Nature* **550**, 469–474 (2017).
14. C. W. Mason, Structural colors in insects. III. *J. Phys. Chem.* **31**, 1856–1872 (1927).
15. E. Shevtsova, C. Hansson, D. H. Janzen, J. Kjærandsen, Stable structural color patterns displayed on transparent insect wings. *Proc. Natl. Acad. Sci. U.S.A.* **108**, 668–673 (2011).
16. U. Stolz, S. Velez, K. V. Wood, M. Wood, J. L. Feder, Darwinian natural selection for orange bioluminescent color in a Jamaican click beetle. *Proc. Natl. Acad. Sci. U.S.A.* **100**, 14955–14959 (2003).
17. B. D. Wilts, A. J. M. Vey, A. D. Briscoe, D. G. Stavenga, Longwing (*Heliconius*) butterflies combine a restricted set of pigmentary and structural coloration mechanisms. *BMC Evol. Biol.* **17**, 226 (2017).
18. S. Berthier, Thermoregulation and spectral selectivity of the tropical butterfly *Prepona meander*: A remarkable example of temperature auto-regulation. *Appl. Phys. A Mater. Sci. Process.* **80**, 1397–1400 (2005).
19. B. R. Wasik *et al*., Artificial selection for structural color on butterfly wings and comparison with natural evolution. *Proc. Natl. Acad. Sci. U.S.A.* **111**, 12109–12114 (2014).
20. S. Kinoshita, S. Yoshioka, Y. Fujii, N. Okamoto, Photophysics of structural color in the *Morpho* butterflies. *Forma Tokyo* **17**, 103–121 (2002).
21. S. Yoshioka, S. Kinoshita, Wavelength-selective and anisotropic light-diffusing scale on the wing of the *Morpho* butterfly. *Proc. Biol. Sci.* **271**, 581–587 (2004).
22. K. Watanabe, T. Hoshino, K. Kanda, Y. Haruyama, S. Matsui, Brilliant blue observation from a *Morpho* butterfly-scale quasi-structure. *Jpn. J. Appl. Phys.* **44**, L48–L50 (2005).
23. R. H. Siddique, S. Diewald, J. Leuthold, H. Hölscher, Theoretical and experimental analysis of the structural pattern responsible for the iridescence of *Morpho* butterflies. *Opt. Express* **21**, 14351–14361 (2013).
24. R. A. Potyrailo *et al*., *Morpho* butterfly wing scales demonstrate highly selective vapour response. *Nat. Photonics* **1**, 123–128 (2007).
25. A. D. Pris *et al*., Towards high-speed imaging of infrared photons with bio-inspired nanoarchitectures. *Nat. Photonics* **6**, 564 (2012).
26. V. Saranathan *et al*., Structure, function, and self-assembly of single network gyroid (I4132) photonic crystals in butterfly wing scales. *Proc. Natl. Acad. Sci. U.S.A.* **107**, 11676–11681 (2010).
27. R. O. Prum, T. Quinn, R. H. Torres, Anatomically diverse butterfly scales all produce structural colours by coherent scattering. *J. Exp. Biol.* **209**, 748–765 (2006).
28. B. D. Wilts, M. A. Giraldo, D. G. Stavenga, Unique wing scale photonics of male Rajah Brooke's birdwing butterflies. *Front. Zool.* **13**, 36 (2016).
29. B. D. Wilts, H. L. Leertouwer, D. G. Stavenga, Imaging scatterometry and microspectrophotometry of lycaenid butterfly wing scales with perforated multilayers. *J. R. Soc. Interface* **6** (suppl. 2), S185–S192 (2009).
30. L. T. Wasserthal, The role of butterfly wings in regulation of body temperature. *J. Insect Physiol.* **21**, 1921–1930 (1975).
31. J. G. Kingsolver, Thermoregulation and flight in *Colias* butterflies: Elevational patterns and mechanistic limitations. *Ecology* **64**, 534–545 (1983).
32. J. T. Munro *et al*., Climate is a strong predictor of near-infrared reflectance but a poor predictor of colour in butterflies. *Proc. R. Soc. B Biol. Sci.* **286**, 20190234 (2019).
33. S. G. Bosi, J. Hayes, M. C. J. Large, L. Poladian, Color, iridescence, and thermoregulation in Lepidoptera. *Appl. Opt.* **47**, 5235–5241 (2008).
34. J. A. Clark, K. Cena, N. J. Mills, Radiative temperatures of butterfly wings. *Z. Angew. Entomol.* **73**, 327–332 (1973).
35. B. Heinrich, Thermoregulation in endothermic insects. *Science* **185**, 747–756 (1974).
36. J. E. Rawlins, Thermoregulation by the black swallowtail butterfly, *Papilio polyxenes* (Lepidoptera: Papilionidae). *Ecology* **61**, 345–357 (1980).
37. H. K. Clench, Behavioral thermoregulation in butterflies. *Ecology* **47**, 1021–1034 (1966).
38. T. C. Bonebrake, C. L. Boggs, J. A. Stamberger, C. A. Deutsch, P. R. Ehrlich, From global change to a butterfly flapping: Biophysics and behaviour affect tropical climate change impacts. *Proc. Biol. Sci.* **281**, 20141264 (2014).
39. G. Nève, C. Hall, Variation of thorax flight temperature among twenty Australian butterflies (Lepidoptera: Papilionidae, Nymphalidae, Pieridae, Hesperiidae, Lycaenidae). *Eur. J. Entomol.* **113**, 571–578 (2016).
40. H. J. MacLean, J. K. Higgins, L. B. Buckley, J. G. Kingsolver, Morphological and physiological determinants of local adaptation to climate in Rocky Mountain butterflies. *Conserv. Physiol.* **4**, cow035 (2016).
41. B. Heinrich, Thoracic temperatures of butterflies in the field near the equator. *Comp. Biochem. Physiol., Part A: Physiol.* **43**, 459–467 (1972).
42. J. R. Howell, M. P. Menguc, R. Siegel, *Thermal Radiation Heat Transfer* (CRC, 2016).
43. A. Herman, C. Vandenbem, O. Deparis, P. Simonis, J. P. Vigneron, Nanoarchitecture in the black wings of *Troides magellanus* : A natural case of absorption enhancement in photonic materials. *Nanophotonic Mater. VIII* **8094**, 80940H (2011).
44. C. C. Tsai *et al*., Butterflies regulate wing temperatures using radiative cooling *Proc. SPIE Int. Soc. Opt. Eng.* **10367**, 103670A (2017).
45. R. De Keyser, C. J. Breuker, R. S. Hails, R. L. H. Dennis, T. G. Shreeve, Why small is beautiful: Wing colour is free from thermoregulatory constraint in the small lycaenid butterfly, *Polyommatus icarus*. *PLoS One* **10**, e0122623 (2015).
46. L. P. Biró *et al*., Role of photonic-crystal-type structures in the thermal regulation of a lycaenid butterfly sister species pair. *Phys. Rev. E Stat. Nonlin. Soft Matter Phys.* **67**, 021907 (2003).
47. Weather Underground, Historical weather for San Pedro Pochutla, Santa María Huatulco, and Deckers. https://www.wunderground.com/history/. Accessed 2 August 2018.
48. Weather Spark, Weather data for Azulillo, Santa María Huatulco, Estes Park, and Perry Park. https://weatherspark.com. Accessed 10 July 2019.
49. B. D. Wilts, A. Matsushita, K. Arikawa, D. G. Stavenga, Spectrally tuned structural and pigmentary coloration of birdwing butterfly wing scales. *J. R. Soc. Interface* **12**, 20150717 (2015).
50. X. Liu, S. Zhang, H. Zhang, Microstructure of butterfly wing scale and simulation of structural color. *Optik* **127**, 1729–1733 (2016).
51. H. Tabata, K. Kumazawa, M. Funakawa, J. I. Takimoto, M. Akimoto, Microstructures and optical properties of scales of butterfly wings. *Opt. Rev.* **3**, 139–145 (1996).
52. L. Wu, Z. Han, Z. Qiu, H. Guan, L. Ren, The microstructures of butterfly wing scales in northeast of China. *J. Bionics Eng.* **4**, 47–52 (2007).
53. F. Pratesi, M. Burresi, F. Riboli, K. Vynck, D. S. Wiersma, Disordered photonic structures for light harvesting in solar cells. *Opt. Express* **21** (suppl. 3), A460–A468 (2013).
54. D. S. Wiersma, P. Bartolini, A. Lagendijk, R. Righini, Localization of light in a disordered medium. *Nature* **390**, 671–673 (1997).
55. K. Chung *et al*., Flexible, angle-independent, structural color reflectors inspired by *Morpho* butterfly wings. *Adv. Mater.* **24**, 2375–2379 (2012).
56. A. Krishna *et al*., Data from "Butterfly thermoregulation." Open Science Framework, 10.17605/OSF.IO/F8RN7. Deposited 20 November 2019.

57. H. O. McMahon, Thermal radiation from partially transparent reflecting bodies. *J. Opt. Soc. Am.* **40**, 376 (1950).
58. S. Catalanotti *et al*., The radiative cooling of selective surfaces. *Sol. Energy* **17**, 83–89 (1975).
59. A. P. Raman, M. A. Anoma, L. Zhu, E. Rephaeli, S. Fan, Passive radiative cooling below ambient air temperature under direct sunlight. *Nature* **515**, 540–544 (2014).
60. J.-l. Kou, Z. Jurado, Z. Chen, S. Fan, A. J. Minnich, Daytime radiative cooling using near-black infrared emitters. *ACS Photonics* **4**, 626–630 (2017).
61. A. Krishna, J. Lee, Morphology-driven emissivity of microscale tree-like structures for radiative thermal management. *Nanoscale Microscale Thermophys. Eng.* **22**, 124–136 (2018).
62. M. G. Moharam, T. K. Gaylord, Rigorous coupled-wave analysis of planar-grating diffraction. *J. Opt. Soc. Am.* **71**, 811 (1981).
63. S. Peng, G. M. Morris, Efficient implementation of rigorous coupled-wave analysis for surface-relief gratings. *J. Opt. Soc. Am. A Opt. Image Sci. Vis.* **12**, 1087–1096 (1995).
64. D. E. Azofeifa, H. J. Arguedas, W. E. Vargas, Optical properties of chitin and chitosan biopolymers with application to structural color analysis. *Opt. Mater.* **35**, 175–183 (2012).
65. W. E. Vargas, D. E. Azofeifa, H. J. Arguedas, Índices de refracción de la quitina, el quitosano y el ácido úrico con aplicación en análisis de color estructural. *Opt. Pura y Apl.* **46**, 55–72 (2013).
66. A. Taflove, S. C. Hagness, *Computational Electrodynamics: The Finite-Difference Time-Domain Method* (Artech House, 2005).
67. M. Sala-Casanovas, A. Krishna, Z. Yu, J. Lee, Bio-inspired stretchable selective emitters based on corrugated nickel for personal thermal management. *Nanoscale Microscale Thermophys. Eng.* **23**, 173–187 (2019).
68. C. D. Ferris, F. M. Brown, *Butterflies of the Rocky Mountain States* (University of Oklahoma Press, 1981).
69. J. Llorente-Bousquets, H. Descimon, K. Johnson, Taxonomy and biogeography of *Archaeoprepona demophoon* in Mexico, with description of a new subspecies (Lepidoptera: Nymphalidae: Charaxinae). *Trop. Lepid.* **4**, 31–36 (1993).
70. Gobierno de México, Información climatológica por estado, Coordinación General del Servicio Meteorológico Nacional. https://smn.conagua.gob.mx/es/informacion-climatologica-por-estado?estado=oax. Accessed 14 November 2019.
71. National Climate Data Center, Supplemental monthly temperature normals for Cheesman, Colorado. https://www.ncdc.noaa.gov/normalsPDFaccess/. Accessed 14 November 2019.
72. J. S. Tsuji, J. G. Kingsolver, W. B. Watt, Thermal physiological ecology of *Colias* butterflies in flight. *Oecologia* **69**, 161–170 (1986).
73. H. Van Dyck, E. Matthysen, Thermoregulatory differences between phenotypes in the speckled wood butterfly: Hot perchers and cold patrollers? *Oecologia* **114**, 326–334 (1998).
74. L. P. Brower, E. H. Williams, L. S. Fink, R. R. Zubieta, M. I. Ramírez, Monarch butterfly clusters provide microclimate advantages during the overwintering season in Mexico. *J. Lepid. Soc.* **62**, 177–188 (2008).
75. F. P. Incropera, D. P. DeWitt, T. L. Bergman, A. S. Lavine, *Fundamentals of Heat and Mass Transfer* (John Wiley, 2006).